RAA 2016 Vol. **16** No. **11**, 169 (6pp) doi: 10.1088/1674–4527/16/11/169

http://www.raa-journal.org *http://iopscience.iop.org/raa*

***R**esearch in*
***A**stronomy and*
***A**strophysics*

On the reality of broad iron L lines from the narrow line Seyfert 1 galaxies 1H0707–495 and IRAS 13224–3809

Pramod Karbhari Pawar[1]*, Gulab Chand Dewangan[2], Madhav Khushalrao Patil[1], Ranjeev Misra[2] and Sharada Keshav Jogadand[1]

[1] S. R. T. M. University, Nanded – 431 606, India; *pawar.pk123@gmail.com*
[2] Inter-University Center for Astronomy and Astrophysics, Pune – 411 007, India

Received 2016 May 2; accepted 2016 July 7

Abstract We performed time resolved spectroscopy of 1H0707–495 and IRAS 13224–3809 using long *XMM-Newton* observations. These are strongly variable narrow line Seyfert 1 galaxies and show broad features around 1 keV that have been interpreted as relativistically broad Fe Lα lines. Such features are not clearly observed in other active galactic nuclei despite sometimes having high iron abundance required by the best fitted blurred reflection models. Given the importance of these lines, we explore whether the rapid variability of spectral parameters may introduce broad bumps/dips artificially in the time averaged spectrum, which may then be mistaken as broadened lines. We tested this hypothesis by performing time resolved spectroscopy using long ($>$100 ks) *XMM-Newton* observations and by dividing them into segments with typical exposures of a few ks. We extracted spectra from each such segment and modeled them using a two component phenomenological model consisting of a power law to represent the hard component and a black body to represent the soft emission. As expected, both the sources showed variations in the spectral parameters. Using these variation trends, we simulated model spectra for each segment and then co-added to get a combined simulated spectrum. In the simulated spectra, we found no broad features below 1 keV and in particular no deviation near 0.9 keV as seen in the real averaged spectra. This implies that the broad Fe Lα line that is seen in the spectra of these sources is not an artifact of the variation of spectral components and, hence, provides evidence that the line is indeed genuine.

Key words: galaxies: general — galaxies: active — galaxies: individual (1H0707–495, IRAS 13224–3809)

1 INTRODUCTION

Active galactic nuclei (AGNs) are thought to be powered by the accretion of matter onto a central supermassive black hole (SMBH). The surrounding matter forms an optically thick, geometrically thin disk that mainly radiates in the optical/ultraviolet region. The broadband X–ray spectrum of an AGN follows a power law shape and is thought to originate from the Compton up-scattering of low energy disk photons by the relativistic electron cloud present in the hot Comptonizing corona (Shapiro et al. 1976; Zdziarski 1985; Sunyaev & Titarchuk 1980; Haardt & Maraschi 1991). The geometry and origin of this corona is, however, still unclear. In addition to this primary power law continuum, several other features are also apparent, which include reflection hump in the energy range 10–50 keV, a broad and skewed Fe Kα fluorescent line around 6.4 keV and soft excess emission below 1 keV. The origin of the reflection hump and the fluorescent Fe Kα line is generally attributed to the reflection of the power law photons by the relatively cold accretion disk (George & Fabian 1991). The first clear evidence for the presence of an extremely broad, skewed iron line came from the *ASCA* long observation of MCG–6–30–15 (Tanaka et al. 1995). Similar line profiles were later noticed in several other AGNs (for a review, see Miller 2007 and references therein). Detection of the broad Fe Kα is important because it carries a signature of the inner accretion disk close to the SMBH, e.g. the line energy tells us the ionization state of the disk, and the inner radius of the accretion disk can be inferred from the redward wing of the line which sometimes even extends down to $\sim$ 2 keV. The line also provides a unique tool to test and verify the theory of general relativity (Fabian et al. 2000).

As mentioned earlier, the AGN spectrum consists of features like soft excess emission, reflection hump and broad Fe K lines. These features can be reproduced using the blurred reflection of the primary continuum from a partially ionized accretion disk (George & Fabian 1991). Several versions of self–consistent reflection models are available, e.g. $reflionx$, $relxill$, etc., which provide a good approximation to the observed data (Ross & Fabian 2005; Crummy et al. 2006; García et al. 2014). Assuming

lamp–post geometry, the recent blurred reflection models describe both the spectral shape and the observed variability of iron lines (Miniutti et al. 2003; Fabian et al. 2004; Zoghbi et al. 2010; Parker et al. 2014b; Gallo et al. 2015). AGN X–ray spectra, however, can also be fitted using a complex partial–covering absorption model which requires the central engine to be obscured by complex absorbing clouds/zones having varying column density, covering fraction and ionization. Here, the observed spectral variability is attributed to the motions of these absorbing clouds (Miller et al. 2008; Turner & Miller 2009; Mizumoto et al. 2014; Marinucci et al. 2014; Parker et al. 2014a).

Both the blurred reflection and partial covering absorption models provide statistically comparable spectral fits and hence must be judged based on the best fit spectral parameter values. One of the key fitting parameters in the reflection scenario is iron abundance. Observationally, many AGNs require overabundance of iron relative to the solar value, e.g. Ark 120 (Matt et al. 2014); NGC 1365 (Walton et al. 2010); 1H0707–495 (Fabian et al. 2009). This overabundance of iron must also produce the accompanying Fe Lα which has not been observed in those AGN spectra. These anomalies cast shadows on the reality of the iron lines and hence on the reflection scenario. Recently, the accompanying Fe Lα line was detected in two extreme cases of typical narrow line Seyfert 1 (NLS1) galaxies, 1H0707–495 and IRAS 13224–3809, using *XMM-Newton* data by Fabian et al. (2009) and Ponti et al. (2010), respectively. In fact, Fabian et al. (2009), examining the Fe Lα line, claimed a lag of 30 s between the direct power law component (1–4 keV) and the reflection component (0.3–1 keV) because it provided better statistics compared to the Kα line. However, the AGN spectrum can be complex due to the presence of a multi–component absorber and soft X–ray excess, and strong spectral variability may introduce artificial spectral features in the mean spectrum. Artifacts in an AGN spectrum introduced due to spectral modeling have been reported earlier, e.g. the soft excess is an artifact of the deficit of emission due to smeared wind absorption while the complex partial-covering absorption model can mimic the broad Fe Kα line quite well. Both of these artifacts are model dependent. The X–ray spectrum of NLS1 is variable and can vary within a few ks (Boller et al. 1996). In the case of *XMM-Newton* observations, where typical exposure time is $>$100 ks, it is very likely that both the flux and spectral shape may change significantly. These changes in the flux and/or spectral parameters may introduce broad bumps/dips in the time averaged spectrum. In this paper, using a two component phenomenological model and time resolved spectroscopy, we try to comment on the reality of the Fe Lα line observed in these two AGNs.

The observational details and data reduction techniques are summarized in Section 2. The spectral analysis and related results are presented in Section 3. The discussion and conclusion are given in Section 4.

2 OBSERVATIONS AND DATA REDUCTION

1H0707–495 has been observed with *XMM-Newton* (Jansen et al. 2001) on various occasions. In particular, continuous observations were carried out during 2008 January 29–February 6 and 2010 September 13–19. We studied all four long observations from 2008 during which the European Photon Imaging Camera–pn (EPIC–pn; Strüder et al. 2001) was operated in large window imaging mode with medium filter while the optical monitor (OM; Mason et al. 2001) was operated with the UVW1 filter in fast imaging mode and $\sim$ 300 exposures were taken during the monitoring. The second source, IRAS 13224–3809, was observed with *XMM-Newton* four times during 2011 July 19–29 for more than 500 ks and once on 2002 January 19 for $\sim$ 64 ks. We used four 2011 observations for the current study in which the OM was operated in fast imaging mode with the UVM2 filter, producing $\sim$ 120 exposures. The EPIC–pn camera was operated in large window imaging mode. We performed time resolved spectroscopy using these observations and found consistency in the results derived from them. Hence, in this paper we present results of 1H0707–495 and IRAS 13224–3809 obtained from observation IDs 0511580101 and 0673580201, respectively. The choice of presenting the results from these observation IDs is mainly driven by having the maximum net useful X–ray exposure time and total number of OM frames. We acquired the Observation Data Files (ODFs) for both sources from the *HEASARC*[1] archive. The datasets were reprocessed and filtered using the *XMM-Newton* Science Analysis System SASv13.5[2] with the latest calibration files and following the SAS ABC guide[3].

To produce calibrated X–ray images, we reprocessed both datasets using the *epproc* pipeline script. *epproc* operates in such a way that it rejects invalid events, determines a good time interval and assigns various flags to each event. It also applies corrections due to the charge transfer inefficiency (CTI) and gain variations. We considered good quality single and double events by setting *FLAG* = 0 and *PATTERN* $\leq$ 4. By generating background light curves above 10 keV, each dataset was examined for the flaring particle background. The time when the data were severely affected by such background flaring was filtered appropriately. The observations were not affected by pile–up and thus no correction was applied. We generated the background corrected source light curves in the soft (0.3–1 keV) and hard (1.5–5 keV) bands which are shown in Figure 1. These light curves show significant variability with fractional variability amplitude of 33 and 56 per cent for 1H0707–495 and 52 and 57 per cent that for IRAS 13224–3809 in soft and hard bands, respectively. *Lower panels* of Figure 1 show variations in the hardness ratio between the two X–ray bands. Variations in the hardness

[1] *http://heasarc.gsfc.nasa.gov/cgi-bin/W3Browse/w3browse.pl*

[2] *http://xmm.esac.esa.int/external/xmm_data_analysis/*

[3] *http://xmm_newton.abc-guide*

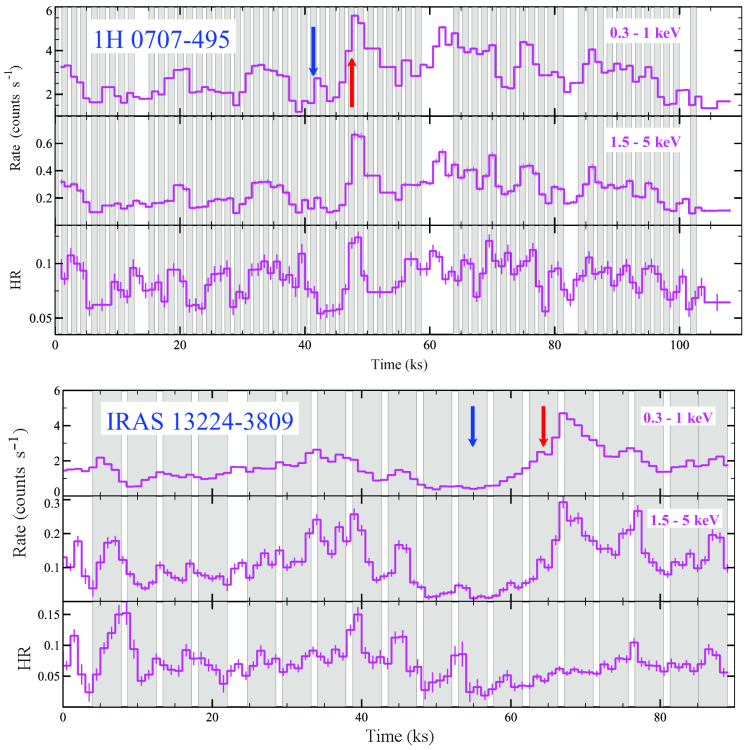

Fig. 1 Background corrected EPIC–pn light curves of 1H0707–495 (*top*) and IRAS 13224–3809 (*bottom*) depicting variations in the 0.3–1 keV soft band (*upper panels*), 1.5–5 keV hard band (*middle panels*) and hardness ratio (*lower panels*). All the light curves are binned in 1 ks bins. The gray shaded areas indicate small exposures used for generating segment spectra. The arrows show the exposures used for the generating the spectra shown in Fig. 2 with similar color.

ratio naturally demonstrate the spectral variations of the source. Due to these short–term variations in the hardness ratio we divided both observations into smaller segments using the time stamps of the simultaneous OM frames. The typical exposure of each X–ray segment was $\sim$ 1.2 ks for 1H0707–495 and 4 ks for IRAS 13224–3809. From each such segment the source spectrum was accumulated from a circular region with radius $35'' - 40''$ centered on the source, whereas the background was extracted from the source free region on the same chip. In Figure 2 we plot two such segment spectra of each source (shown by arrows with similar colors in Figure 1) to demonstrate the spectral variations. The spectra were unfolded by fitting a *power law* model with Γ fixed at 2. This again shows the spectral variations between the segments. The EPIC–pn response files, i.e. the redistribution matrix files (RMF) and the effective area files (ARF), were generated using the SAS tasks *rmfgen* and *arfgen*, respectively. The resulting spectra were then grouped using the *FTOOL* task *grppha* to a minimum of 20 counts per spectral bin so that the χ^2 minimization technique could be employed. All of the errors in the best-fit parameters quoted here correspond to the 1–σ range.

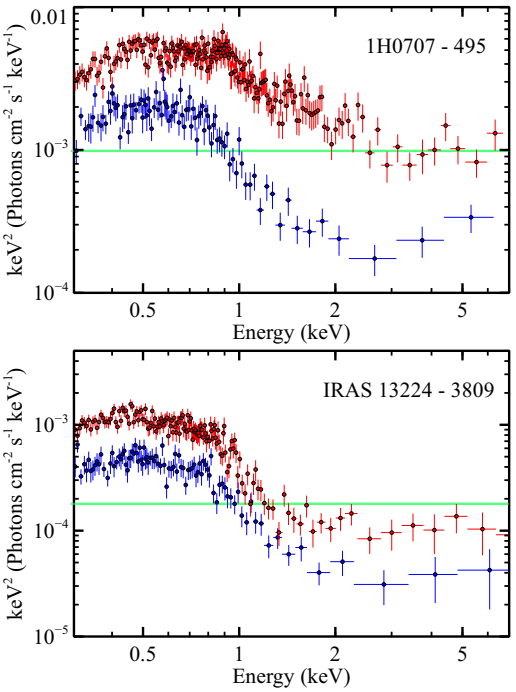

Fig. 2 The unfolded EPIC–pn spectra derived from two segments of the 1H0707–495 (*top*) and IRAS 13224–3809 (*bottom*). These spectra were unfolded with a power law model having Γ fixed at 2 to demonstrate the spectral variation within the observations for both AGNs.

3 SPECTRAL ANALYSIS

The X–ray spectrum of an AGN, particularly of an NLS1 case, is considered to be a two component spectrum repre-

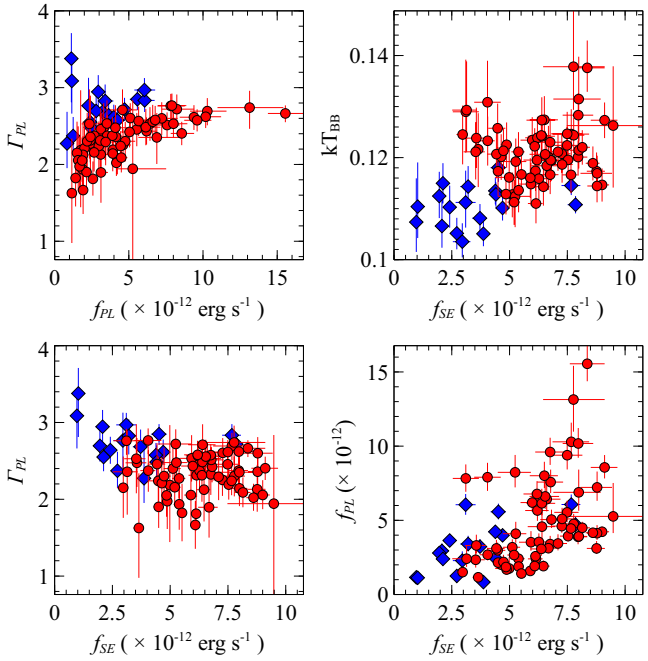

Fig. 3 Short–term variation of spectral parameters derived from 100 ks long observations of 1H0707–495 (*red circles*) and IRAS 13224–3809 (*blue diamonds*). The component fluxes, f_{SE} and $f_{\rm PL}$, are derived from 0.3–1 keV and 1.5–3 keV bands, respectively.

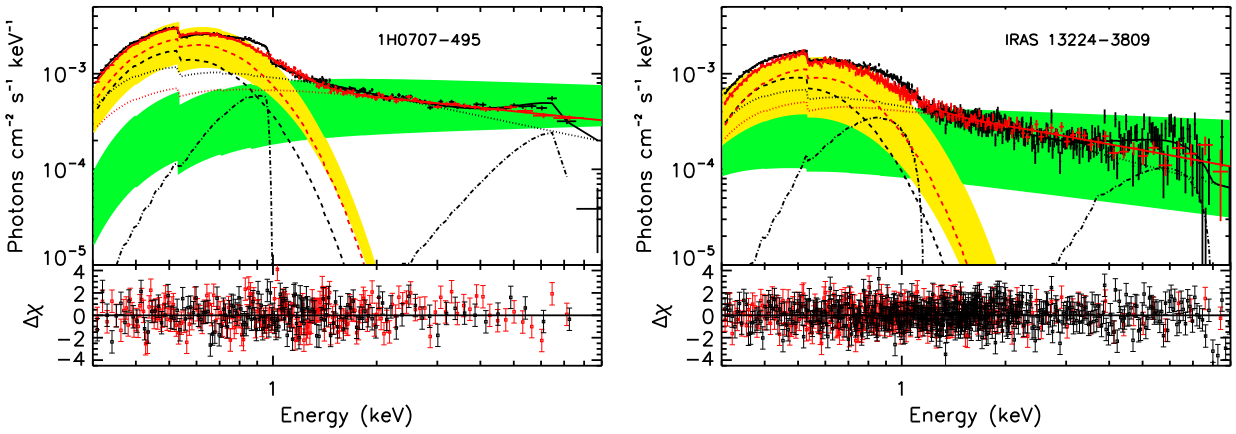

Fig. 4 The unfolded time averaged spectrum (*in black*) and simulated spectrum (*in red*) of 1H0707–495 (*top*) and IRAS 13224–3809 (*bottom*) were fitted with an absorbed PL (*dotted lines*) and BB (*dashed lines*) components. Two *Laor* lines (*dash-dotted line*) are used to model the broad Fe lines. χ variation is shown in the bottom panel of each figure. The solid thick lines are the best fit model. The green and yellow shaded regions display the area between the lowest and highest flux values of PL and BB components, respectively. The figure for 1H0707–495 is rebinned for clarity.

senting hard/primary emission and soft emission. To model the spectra generated from each X–ray segment, we used a two component phenomenological model (*powerlaw + bbody*) corrected for Galactic absorption, with a power law (PL) component to constrain the continuum or hard emission and a black body (BB) component to represent the soft emission (SE). We fitted the entire 0.3–10 keV band with the *wabs*(powerlaw + bbody)* model. The component fluxes were calculated using the $cflux$ model. We noted the best fit values of photon index, disk temperature and component fluxes (f_{SE} in 0.3–1 keV and $f_{\rm PL}$ in 1.5–3 keV bands). Due to the poor signal above 6 keV we could not constrain the Fe Kα line in both objects and, therefore, we fitted spectra without a line component. The detailed results of this time resolved spectroscopy will be presented in a separate paper (Pawar et al., in preparation), which will discuss both the spectral variability as well as the X–ray/optical correlation. For the sake of brevity, here we describe the quality of fits and the observed variations. Most of the spectra were fitted well using a two component model resulting in the reduced χ^2 between 0.8–1.2. Any fit whose reduced χ^2 lies outside of these values was

Table 1 Best fit spectral results for 1H0707–495 and IRAS 13224–3809. The best fit model for the average spectra is *wabs*(powerlaw+bbody+laor+laor)* while for the simulated spectra it is *wabs*(powerlaw+bbody)*.

	1H0707–495		IRAS 13224–3809	
Parameter	Average Spectrum	Simulated Spectrum	Average Spectrum	Simulated Spectrum
Exposure	95 ks	61 ks	83 ks	40 ks
Net Count Rate	3.5 ± 0.1	3.4 ± 0.1	1.9 ± 0.1	1.8 ± 0.1
$N_{\rm H}$ ($\times 10^{20}$ cm $^{-2}$)	$5.9^{+0.2}_{-0.2}$	$5.1^{+0.2}_{-0.2}$	$5.3^{+0.2}_{-0.2}$	$5.4^{+0.3}_{-0.3}$
Γ	$2.76^{+0.03}_{-0.02}$	$2.4^{+0.02}_{-0.02}$	$2.94^{+0.04}_{-0.04}$	$2.66^{+0.04}_{-0.04}$
$A_{\rm PL}$ ($\times 10^{-4}$)	$10.5^{+0.2}_{-0.1}$	$7.6^{+0.1}_{-0.1}$	$5.2^{+0.1}_{-0.1}$	$4.6^{-0.1}_{-0.1}$
kT (eV)	108^{+1}_{-1}	122^{+1}_{-1}	96^{+3}_{-4}	109^{+1}_{-1}
$A_{\rm BB}$ ($\times 10^{-5}$)	$7.2^{+0.2}_{-0.2}$	$8.4^{+0.2}_{-0.2}$	$4.0^{+0.2}_{-0.2}$	$4.4^{+0.2}_{-0.2}$
$E_{\rm K\alpha}$ (keV)	$6.65^{+0.05}_{-0.05}$	–	$7.43^{+0.27}_{-0.26}$	–
Index (β) [a]	$3.65^{+0.08}_{-0.11}$	–	$5.1^{+0.3}_{-0.3}$	–
$R_{\rm in}$ (R_g) [a]	< 1.7	–	$1.77^{+0.08}_{-0.11}$	–
$R_{\rm out}$ (R_g) [a]	400*	–	400*	–
Inclination (degree) [a]	30*	–	30*	–
f_{K_α} [b] ($\times 10^{-5}$)	$2.28^{+0.27}_{-0.21}$	–	$1.4^{+0.2}_{-0.1}$	–
$E_{\rm L\alpha}$ (keV)	$0.92^{+0.01}_{-0.01}$	–	$1.1^{+0.1}_{-0.1}$	–
f_{L_α} [b] ($\times 10^{-4}$)	$4.86^{+0.31}_{-0.25}$	–	$3.66^{+0.68}_{-0.51}$	–
χ^2 / dof	489 / 342	314 / 284	351 / 350	238 / 243

Notes: (a) signifies line parameters that are tied between Fe L and Fe K lines and (b) indicates line flux in units of photons cm^{-2} s^{-1}.

termed a bad fit and was not considered in further analysis. This resulted in a total of 68 and 19 spectra from single observations for 1H0707–495 and IRAS 13224–3809, respectively. From this study, it has been observed that both the PL and SE components are variable. Figure 3 shows the intra–observation variability of spectral parameters of both components for 1H0707–495 (red circles) and IRAS 13224–3809 (blue diamonds). From the $\Gamma_{\rm PL}$ - $f_{\rm PL}$ plot, both objects follow the softer when brighter nature. This nature was already studied by Sobolewska & Papadakis (2009) using *RXTE* data from a sample of 10 Seyfert galaxies and found that except for NGC 5548 all other AGNs showed softer when brighter behavior. However, using 24 galaxies from the Palomer sample observed by *Swift*, Connolly et al. (2016) showed that the high luminosity AGNs appeared softer when brighter while low luminosity AGNs showed a harder when brighter trend. Both objects studied here are NLS1s with a high accretion rate indicating that they exhibit similar spectral properties as high luminosity end AGNs. Variability of these spectral parameters on a shorter timescale may introduce artifacts in the time averaged spectrum over sufficiently longer time. Such averaging may lead to bumps and dips in the time averaged spectrum causing artificial broad line like features. To check this possibility, we generated simulated data with the best fit theoretical model of each segment spectra using the *XSPEC* task *fakeit*. Later, the resultant simulated spectra were co-added together using the *FTOOL addascaspec* to get the combined simulated spectrum. The response and background files were also merged together. The resultant combined simulated spectra of both objects were used for further spectral analysis. Similarly, we also derived the time averaged spectra from the $35''$ region centered on the source position as well as the background spectra from a region devoid of source contamination. The resultant spectra were grouped so that the χ^2 minimization technique could be applied.

We applied our phenomenological model to the simulated spectra and average spectra simultaneously. The simulated spectra of both objects provided excellent fits with no apparent deviations from the model, however, the fit to the average spectra was very poor and showed large deviations. To account for these deviations we added two *Laor* components. Assuming that the origin of both the lines is same, we tied the emissivity index (β), inner radius ($R_{\rm in}$), outer radius ($R_{\rm out}$) and inclination of both the *Laor* components to each other. The spectral results for both objects are shown in Table 1. The difference in the best fit PL and BB parameters for simulated and time averaged spectra as seen in Table 1 is probably due to the fact that the good time interval (GTI) of simulated spectra is a subset of GTI of average spectra. This extra time in the average spectrum might have changed the shape of the spectrum. Figure 4 displays our best fit spectral results. For each of the sources, we plotted the data along with the best fit model and the variation of χ for both the simulated spectra (red) and the average spectra (black). The individual model components of PL (dotted lines), BB (dashed lines) and two *Laor* (dot-dashed) lines are also shown. From the figure it is clear that the simulated spectrum does not require the *Laor* line at $\sim$ 1 keV. The green and yellow shaded regions indicate the range of variability of PL and BB normalizations, respectively.

4 DISCUSSION AND CONCLUSION

We performed time resolved spectroscopy of NLS1 galaxies 1H0707–495 and IRAS 13224–3809 using $\sim$ 100 ks

long *XMM-Newton* observations. NLS1 galaxies are generally characterized by a steep PL spectrum and rapid variability. We found that both these AGNs show strong short–term variations during the observations. Figure 1 shows significant variability observed in the soft band (0.3–1 keV), the hard band (1.5–5 keV) and in the hardness ratio. The variability in hardness ratio suggests spectral variability within the observation. These spectral variations motivated us to study the variability of spectral components and the artifacts which could be introduced by such variability in the average spectrum. In this study we performed time resolved spectroscopy by generating spectra from multiple small segments. In Figure 2 we show unfolded spectra of two typical segments fitted with a PL model (with Γ fixed at 2) to show the short–term spectral variations in both the sources. This figure reveals the significant spectral variability within the observation. We find that each segment spectrum can be easily modeled using a two component model (PL+BB) modified by Galactic absorption. As expected, our spectral results demonstrate that all of the spectral parameters were variable and are plotted in Figure 3. The variability of $\Gamma_{\rm PL}$ and $kT_{\rm BB}$ indicates that the observed variability is not just due to flux variations but that the spectral shape is also changing.

The best fit model for each spectrum was used to simulate data which were co–added to get the combined simulated spectra. These combined simulated spectra were later compared with the actual time averaged spectra. The result of this spectral fitting is tabulated in Table 1. The spectral parameters show variations between the simulated and average spectra, which are solely because the GTI of simulated spectra is a subset of total exposure of the time averaged spectra. The extra time in the average spectra caused the variation in the spectral parameters seen in Table 1. We find that the time averaged spectra showed significant deviations and required additional line components and, therefore, we added two $Laor$ lines to the model. In the simulated spectra we do not see a line at 6.4 keV because our initial model did not incorporate the line model, however, no deviation was seen near 0.9 keV. This suggests that the line we see in the time averaged spectra is not an artifact of the variation of spectral components. In fact, there is no deviation near 0.9 keV, which is an independent way of demonstrating that the line indeed is a genuine feature. Even if we did not find a line feature but rather observed a positive deviation around 0.9 keV, we would have certainly lowered the overabundance required in these objects and would have improved the current reflection models.

Acknowledgements We thank the anonymous referee for his/her constructive comments. PKP acknowledges financial support from CSIR, New Delhi. SKJ acknowledges financial support from DST, New Delhi through the INSPIRE Scheme. This research has made use of observations with the *XMM-Newton* telescope and analysis is carried out using the software provided by Science Analysis System (SAS) and *FTOOL* provided by the High Energy Astrophysics Science Archive Research Center (HEASARC) software package. The first three figures were generated using the *veusz* plotting tool.

References

Boller, T., Brandt, W. N., & Fink, H. 1996, A&A, 305, 53
Connolly, S. D., McHardy, I. M., Skipper, C. J., & Emmanoulopoulos, D. 2016, MNRAS, 459, 3963
Crummy, J., Fabian, A. C., Gallo, L., & Ross, R. R. 2006, MNRAS, 365, 1067
Fabian, A. C., Iwasawa, K., Reynolds, C. S., & Young, A. J. 2000, PASP, 112, 1145
Fabian, A. C., Miniutti, G., Gallo, L., et al. 2004, MNRAS, 353, 1071
Fabian, A. C., Zoghbi, A., Ross, R. R., et al. 2009, Nature, 459, 540
Gallo, L. C., Wilkins, D. R., Bonson, K., et al. 2015, MNRAS, 446, 633
García, J., Dauser, T., Lohfink, A., et al. 2014, ApJ, 782, 76
George, I. M., & Fabian, A. C. 1991, MNRAS, 249, 352
Haardt, F., & Maraschi, L. 1991, ApJ, 380, L51
Jansen, F., Lumb, D., Altieri, B., et al. 2001, A&A, 365, L1
Marinucci, A., Matt, G., Miniutti, G., et al. 2014, ApJ, 787, 83
Mason, K. O., Breeveld, A., Much, R., et al. 2001, A&A, 365, L36
Matt, G., Marinucci, A., Guainazzi, M., et al. 2014, MNRAS, 439, 3016
Miller, J. M. 2007, ARA&A, 45, 441
Miller, L., Turner, T. J., & Reeves, J. N. 2008, A&A, 483, 437
Miniutti, G., Fabian, A. C., Goyder, R., & Lasenby, A. N. 2003, MNRAS, 344, L22
Mizumoto, M., Ebisawa, K., & Sameshima, H. 2014, PASJ, 66, 122
Parker, M. L., Walton, D. J., Fabian, A. C., & Risaliti, G. 2014a, MNRAS, 441, 1817
Parker, M. L., Wilkins, D. R., Fabian, A. C., et al. 2014b, MNRAS, 443, 1723
Ponti, G., Gallo, L. C., Fabian, A. C., et al. 2010, MNRAS, 406, 2591
Ross, R. R., & Fabian, A. C. 2005, MNRAS, 358, 211
Shapiro, S. L., Lightman, A. P., & Eardley, D. M. 1976, ApJ, 204, 187
Sobolewska, M. A., & Papadakis, I. E. 2009, MNRAS, 399, 1597
Strüder, L., Briel, U., Dennerl, K., et al. 2001, A&A, 365, L18
Sunyaev, R. A., & Titarchuk, L. G. 1980, A&A, 86, 121
Tanaka, Y., Nandra, K., Fabian, A. C., et al. 1995, Nature, 375, 659
Turner, T. J., & Miller, L. 2009, A&A Rev., 17, 47
Walton, D. J., Reis, R. C., & Fabian, A. C. 2010, MNRAS, 408, 601
Zdziarski, A. A. 1985, ApJ, 289, 514
Zoghbi, A., Fabian, A. C., Uttley, P., et al. 2010, MNRAS, 401, 2419